Sustainable Chemical Engineering
https://ojs.wiserpub.com/index.php/SCE/

UNIVERSAL WISER PUBLISHER

Research Article

Influence of Carbon Chain Length of Silicates on Visible Light Transmittance and Infrared Light Transmittance of Photovoltaic Glass

Sun Guodong[1,3*], Tian Yonggang[2], Ma Yingfei[1,3], Chen Shaodi[1], Wang Xinqi[1], Guo Zihou[1], Zhang Linjie[3], Zhang Wei[1], Lin Yuanzhi[1]

[1]Materials and Packaging Engineering, Fujian Polytechnic Normal University, Fuzhou, 350300, China
[2]Xinfuxing Glass (Fujian) Co, Ltd. Fuzhou, 350002, China
[3]State Key Laboratory of Structural Chemistry Fujian Institute of Research on the Structure of Matter, Chinese Academy of Sciences, Fuzhou, 350002, China
E-mail: sunguodong20@mails.ucas.ac.cn

Received: 9 September 2025; **Revised:** 10 November 2025; **Accepted:** 12 November 2025

Abstract: To address Photovoltaic (PV) glass solar energy loss (reflection) and efficiency degradation induced by infrared light absorption (which causes increased battery temperature and thereby exacerbates carrier recombination), this study examines silicate precursors (Tetramethoxysilane (TMOS), Tetraethoxysilane (TEOS), Tetrabutoxysilane (TBOS)) with varying carbon chain lengths on coating performance. X-Ray Diffraction (XRD)/Scanning Electron Microscopy (SEM) characterization results show all coatings are amorphous, but TMOS yields higher crystallinity and denser microstructures; TEOS/TBOS form defective structures via longer chains. Optical tests indicate that all coatings have 90%-96% Visible Light (VL, 300-800 nm) transmittance (TMOS: up to 96%, with the least fluctuation); TMOS has the lowest infrared (IR, 2.5-25 μm) transmittance (~ 40%). In addition, TMOS coatings retain > 90% VL transmittance over 24 months, and TEOS and TBOS show shows ultra-low aging attenuation. These results demonstrate that TMOS is the optimal precursor for preparing high-performance PV glass coatings, which can effectively reduce solar energy loss and mitigate efficiency degradation of PV modules, providing technical support for the development of high-efficiency photovoltaic systems.

***Keywords*:** Photovoltaic glass, silicate coating, carbon chain length, transmittance, stability

1. Introduction

In modern energy supply, sunlight is the most ideal sustainable energy source, providing clean energy for the photovoltaic power generation industry. When light comes into contact with the surface of an object, various reflections occur on the contact surface.[1] However, some unwanted light reflections can bring about adverse consequences.[2] For example, in photovoltaic solar modules, when light enters the solar module from the air, the first surface it encounters is the encapsulated glass of the photovoltaic module.[3] If the incident light generates a large amount of reflection on this surface, the overall power generation efficiency of the photovoltaic module will be greatly reduced, and the utilization rate of solar energy will decrease.[4] Currently, in the energy collection process of solar cells, the light reflection on the surface of the glass cover plate leads to about 8% solar energy loss.[5] Meanwhile, the absorption of light in the infrared

DOI: https://doi.org/10.37256/sce.7120268577

band aggravates the temperature rise of the battery components, which in turn increases the carrier recombination rate of semiconductor materials, reducing the photoelectric conversion efficiency by about 5-10%.[6] This thermal effect caused by infrared absorption will also accelerate the aging of packaging materials and shorten the service life of batteries.[7]

Surface modification technology to prepare anti-reflection films or coatings can effectively reduce the reflection loss of sunlight on the surface of the glass cover plate of optoelectronic devices.[8] At the same time, by regulating the scattering or interference effect of the film structure on infrared light, it can also reduce the absorption rate of infrared light and inhibit the temperature rise of the battery.[9] At the same time, the long-term service cycle of solar panels requires the anti-reflection film to have excellent durability and weather resistance, which is a key factor in ensuring the long-term efficient operation of the battery.[10]

In recent years, low-refractive-index silicon dioxide (SiO_2) has attracted much attention in the research of anti-reflection materials. Researchers have successfully developed multifunctional nano-coating materials with super-wetting properties by optimizing preparation methods and regulating nanostructures, and have made systematic breakthroughs in energy regulation in the infrared band.[11] Through mesoporous pore size regulation (2-50 nm), porosity optimization (40%-70%) and multilayer film structure design, the precise regulation of reflectivity in different infrared bands (near-infrared 700-2,500 nm, mid-infrared 2.5-25 μm) has been realized.[12] However, the composition of most coatings contains various metal elements, which seriously affects the service life of the coatings, especially under high-temperature conditions.[13] Therefore, there is an urgent need to develop non-metallic solar cell glass coatings with high anti-reflection and low infrared absorption.

Here, we investigated the influence of tetramethyl orthosilicate, tetraethyl orthosilicate and tetrabutyl orthosilicate with different alkane structures on the visible light anti-reflection effect and infrared light reflection effect when preparing photovoltaic glass coatings. The research shows that under the same synthesis conditions, tetramethyl orthosilicate with a shorter carbon chain exhibits the best visible light anti-reflection effect and infrared light reflection effect (96% Transmittance). This is because tetramethyl orthosilicate has the shortest carbon chain, and the SiO_2 film formed after hydrolysis and condensation has less carbon impurities and a more uniform and dense structure. Its refractive index has the best optical matching with visible light anti-reflection and infrared light reflection, so it shows a better light regulation effect. Our research results provide ideas for the synthesis of high-performance anti-reflection coatings for photovoltaic glass.

2. Experiments and methods

2.1 *Material synthesis*

For the preparation of anti-reflective coating solutions, the base solvent (Solution A) was first prepared by weighing 3.24 g of absolute ethanol, 3.24 g of absolute methanol, and 3.24 g of absolute isopropanol into a 50 mL beaker, followed by magnetic stirring at 300 r/min for 2 min at room temperature (25 ± 2 ℃) to obtain a homogeneous mixed solvent, which was stored for subsequent use. Control experiments involved preparing four groups of coating solutions with a total silicon source mass of 4.00 g each. For the TMOS experimental group, 4.00 g of Tetramethyl Orthosilicate (TMOS) and 5.15 g of deionized water were added to a 100 mL round-bottom flask and stirred at 250 r/min for 2 min at room temperature to yield the silicon source precursor (Solution B1). Solution A was then slowly added into Solution B1, followed by continuous stirring at room temperature for 1 min. The flask was subsequently placed in a 70 ± 1 ℃ water bath and stirred at 300 r/min for 10 min, after which 0.50 g of 15 wt% ammonia solution was added and stirred for 30 min. Finally, 0.50 g of glycerol was introduced, followed by 10 min of stirring, and the solution was aged at room temperature for 24 h to obtain the TMOS coating solution. The TEOS and TBOS experimental groups were synthesized similarly by replacing TMOS with equimolar amounts of Tetraethyl Orthosilicate (TEOS) and Tetrabutyl Orthosilicate (TBOS), respectively.

Tetramethyl Orthosilicate (TMOS, ≥ 99%), Tetraethyl Orthosilicate (TEOS, ≥ 98%), Tetrabutyl Orthosilicate (TBOS, ≥ 97%) were purchased from Aladdin Industrial Corp. (Shanghai, China); absolute ethanol (≥ 99.7%), methanol (≥ 99.8%), isopropanol (≥ 99.5%) from Sinopharm Chem. Reagent Co., Ltd. (Beijing, China); 15 wt% ammonia solution (analytical grade) and glycerol (≥ 99.0%) from Macklin Biochemical Tech. Co., Ltd. (Shanghai, China). All reagents were used without further purification.

2.2 *Characteristic*

A variety of testing techniques were employed to systematically characterize the key properties of the prepared anti anti-reflective coating solutions and coated photovoltaic coated photovoltaic glass. The phase structure of the coatings was analyzed using an X-Ray Diffractometer (model XD-3) with Cu Kα radiation, operating over a 2θ scanning range of 10°-80° at a scanning speed of 5°/min; the presence of amorphous structures was determined by identifying characteristic diffraction peaks. The surface morphology and film-substrate bonding state of the coatings were observed using a scanning electron microscope (model ZEISS Sigma 300) at an accelerating voltage of 5.00 kV and a working distance of 7.1-7.8 mm. Samples were sputter-coated with a 5 nm-thick gold layer using an ion sputter coater (Quorum Q150T) for 60 seconds to enhance conductivity before Scanning Electron Microscopy (SEM) observation. Images were captured at magnifications ranging from 5.00 K to 50.00 K to analyze coating coverage, surface defects, and particle arrangement. The transmittance of the coated glass in the 300-800 nm wavelength range was measured using an ultraviolet-visible spectrophotometer (model Shimadzu UV-2700) at a scanning rate of 200 nm/min with a data interval of 1 nm. Additionally, an optical transmittance detector (model Xiamen C&D LH-221) was used to evaluate optical performance via Visible Light Transmittance (VLT) under environmental conditions of 25 ± 2 ℃ and 45 ± 5% relative humidity. Infrared transmittance was tested using an infrared photometer. Environmental aging tests, including UV15 aging, TC200 temperature cycling, 96-hour salt spray, DH1000 damp heat, 400-cycle scrubbing, PCT48 pressure cooking, and HF10 hydrofluoric acid corrosion, were conducted to simulate harsh outdoor conditions. Transmittance was measured using the ultraviolet-visible spectrophotometer before and after these tests, and the attenuation rate was calculated to assess the long-term stability of the coatings. All tests were performed in parallel 3-5 times to ensure data reliability, providing support for analyzing the effects of different silicon source systems on coating properties and optimizing the preparation process.

3. Results and discussion

Figure 1 presents the X-Ray Diffraction (XRD) patterns of coatings fabricated using Tetrabutyl Orthosilicate (TBOS), Tetramethyl Orthosilicate (TMOS), and Tetraethyl Orthosilicate (TEOS). All patterns exhibit broadened diffuse scattering peaks instead of sharp, narrow crystalline diffraction peaks, indicating that the prepared coatings mainly possess an amorphous structure.

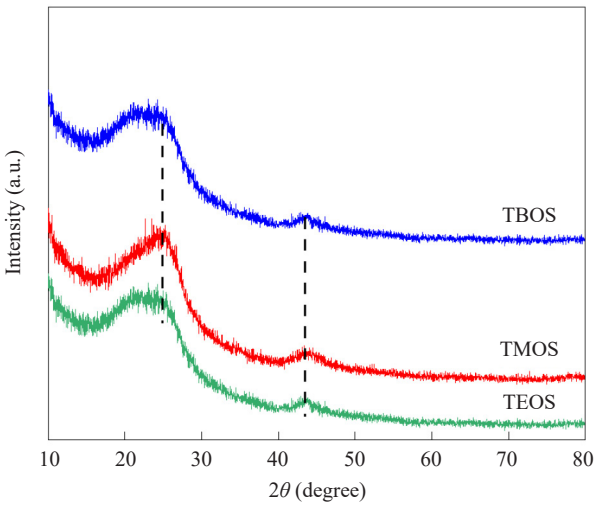

Figure 1. XRD patterns of coatings prepared from tetramethyl orthosilicate, tetraethyl orthosilicate, and tetrabutyl orthosilicate

Notably, the coating prepared from TMOS shows the sharpest XRD peak among the three. This phenomenon

suggests that the TMOS-derived coating has a relatively higher crystallinity. The sharpness of an XRD peak is directly related to the degree of order in the atomic arrangement within the crystal; a sharper peak implies a more regular arrangement of atoms in the lattice. Through quantitative calculation, the relative intensities of the crystallinity peaks for the three substances are approximately as follows: TBOS : TMOS : TEOS ≈ 3.2 : 2.1 : 1.3. Furthermore, this characteristic also reflects that during the preparation process, the hydrolysis and polycondensation reactions of TMOS may proceed more uniformly and stably. Such a stable reaction environment provides favorable conditions for the ordered growth of crystals, ultimately resulting in a coating structure with a regular atomic arrangement.

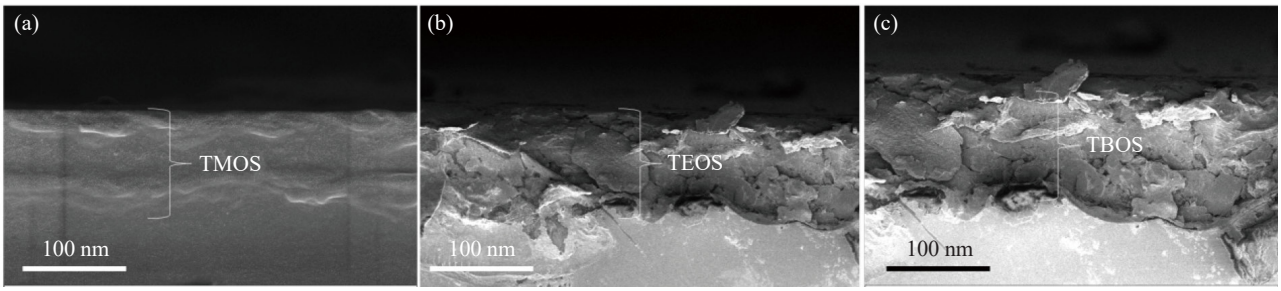

Figure 2. SEM images of coatings prepared from tetramethyl orthosilicate (a), tetraethyl orthosilicate (b), and tetrabutyl orthosilicate (c)

Figure 2 displays the Scanning Electron Microscopy (SEM) images of coatings synthesized using Tetramethyl Orthosilicate (TMOS), Tetraethyl Orthosilicate (TEOS), and Tetrabutyl Orthosilicate (TBOS). The coating prepared from TMOS (Figure 2a) exhibits a smooth, dense, and homogeneous structure with well-defined interlayer boundaries, indicating that TMOS is conducive to the formation of a compact coating. In contrast, the coatings fabricated from TEOS (Figure 2b) and TBOS (Figure 2c) show rough, porous, and fragmented morphologies, with obvious cracks and uneven textures.

This difference in microstructure can be attributed to the carbon chain length of the silicate precursors. The shorter carbon chain of TMOS enables more uniform hydrolysis and polycondensation reactions, thereby forming a stable and dense coating. Meanwhile, the longer carbon chains in TEOS and TBOS may introduce greater steric hindrance or lead to incomplete reactions, resulting in the formation of defective and loose coating structures. Such morphological variations can exert a significant impact on the optical, mechanical, and protective properties of the coatings.

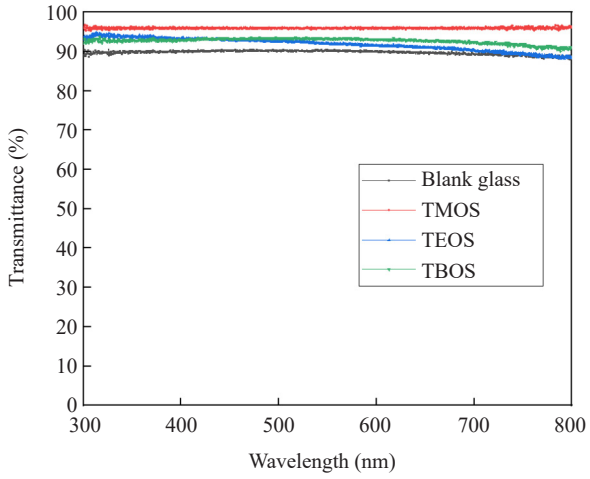

Figure 3. Visible light transmittance of coatings prepared from tetramethyl orthosilicate, tetraethyl orthosilicate, and tetrabutyl orthosilicate

Figure 3 shows the visible light transmittance performance (within the wavelength range of 300-800 nm) of coatings prepared using Tetramethyl Orthosilicate (TMOS), Tetraethyl Orthosilicate (TEOS), and Tetrabutyl Orthosilicate (TBOS). The results indicate that the transmittance of all coated glass samples maintains a high level of 90%-96%, which demonstrates that the three types of coatings have minimal negative impacts on visible light transmittance.

Among them, the TMOS-derived coating exhibits the highest transmittance across the entire visible light band with the smallest fluctuation. This can be attributed to the shortest carbon chain structure of TMOS, which promotes uniform hydrolysis and condensation reactions, leading to the formation of a dense film with well-matched refractive index. This structure effectively reduces the reflection loss of visible light. In contrast, the TEOS and TBOS coatings, due to their longer carbon chains, have more residual carbon impurities from incomplete hydrolysis and poorer film uniformity, resulting in slightly lower transmittance compared to the TMOS group. Particularly, the transmittance of the TBOS coating shows a more obvious decrease in the long-wavelength region of visible light.

Additionally, in the long-wavelength region of 700-800 nm, the differences in transmittance among the various curves are more significant. This reflects that long-wavelength light is more sensitive to the microstructural defects and impurity distribution of the coatings.

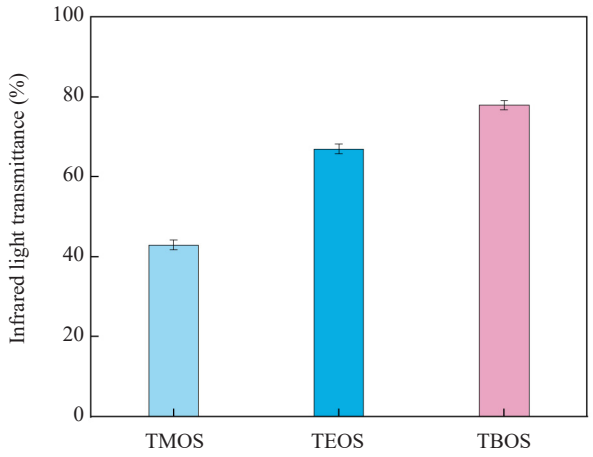

Figure 4. Infrared light transmittance of coatings prepared from tetramethyl orthosilicate, tetraethyl orthosilicate, and tetrabutyl orthosilicate

Figure 4 presents the infrared light transmittance (within the infrared wavelength range of 2.5-25 μm) of coatings fabricated using Tetramethyl Orthosilicate (TMOS), Tetraethyl Orthosilicate (TEOS), and Tetrabutyl Orthosilicate (TBOS). It can be observed that there are significant differences in infrared light transmittance among the coatings prepared with different precursors: the coating derived from TMOS exhibits the lowest infrared light transmittance (approximately 40%), the transmittance of the coating prepared from TEOS is moderately increased (approximately 60%), and the coating made from TBOS shows the highest infrared light transmittance (nearly 80%). This result indicates that the type of precursor has a significant impact on the infrared light transmittance of the coatings, and the carbon chain length of the precursor is likely one of the key factors influencing this property.[14]

Figure 5 presents the variation of visible light transmittance (within the wavelength range of 300-800 nm) for the coating prepared from Tetramethyl Orthosilicate (TMOS) over a 24-month period. The coating underwent a 24-month stability test in a natural environment. The test was conducted on the rooftop of the Experimental Building at Fujian Normal University of Technology, Fuqing City, Fuzhou City, Fujian Province, China, with coordinates 119.377793° E, 25.704034° N. The test period lasted from August 1, 2023, to July 31, 2025. As observed from the figure, the transmittance curves of the coating at different storage durations (1 day, 1 month, 6 months, 12 months, 18 months, and 24 months) are generally consistent and all maintain a high level (approximately above 90%). This indicates that the coating exhibits excellent stability over the 24-month time span-with no significant decrease in transmittance occurs due to long-term storage. After being exposed to natural conditions for 24 months, the light transmittance of the material in

the range of 700-800 nm decreased slightly. This phenomenon may be attributed to the long-term aging, which leads to the peeling of the anti-reflective coating on the glass surface. Such performance demonstrates that the coating can retain its optical properties in the visible light region for an extended period, thereby possessing favorable durability.

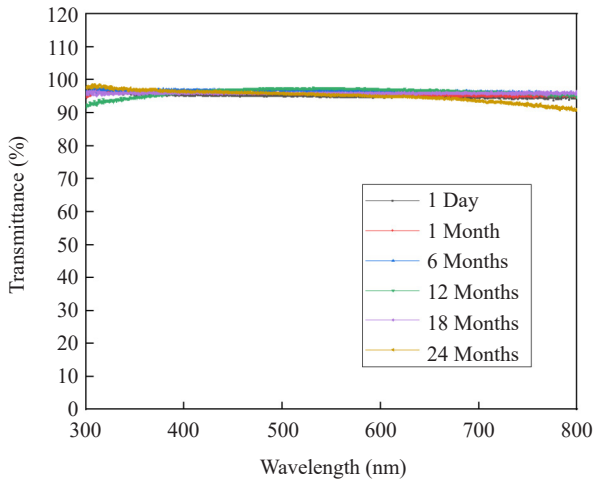

Figure 5. Visible light transmittance of the coating prepared from Tetramethyl Orthosilicate (TMOS) over 24 months

Table 1. Test attenuation rates under different environmental aging conditions

Environmental aging test type	Effective transmission ratio attenuation rate of solar light/%
HF10	0.80
DH1000	0.72
TC200	0.12
UV15	0.02
PCT48	0.63
Salt mist 96 h	0.23
Rinse 400 time	0.32
Acid rain corrosion	0.35
Dust abrasion	0.88

The glass with TMOS was tested under simulated aging conditions, and the test results are presented in Table 1. The definitions of the aging test types are as follows: HF10 refers to a "Humidification-Freezing" aging test, where "10" represents the number of cycles or test duration; DH1000 denotes a "Damp Heat (DH)" test, with "1,000" indicating the test duration; TC200 stands for a "Temperature Cycling (TC)" test, where "200" is the number of cycles; UV15 corresponds to an "Ultraviolet (UV)" aging test, with "15" representing the UV irradiation dose or test duration; and PCT48 refers to a "Pressure Cooker Test (PCT)", where "48" signifies the test duration (48 hours). Among the tests, the attenuation rate of the effective transmittance under the UV15 test was only 0.02%, demonstrating extremely strong stability of light transmittance performance. The attenuation rates under the TC200 test and 96-hour salt spray test were 0.12% and 0.23%, respectively, which also remained at a low attenuation level. The attenuation rate after 400

scrubbing cycles was 0.32%, while the attenuation rates under the DH1000 and PCT48 tests were both 0.63%, and that under the HF10 test was 0.80%. Acid rain corrosion simulates acidic rainfall environments (usually pH < 5.6) to assess the coating's resistance to acidic media like sulfuric and nitric acids, with a 0.35% solar light effective transmission ratio attenuation rate indicating good acid resistance, while dust abrasion mimics sandy conditions by using high-speed dust particles to test the coating's scratch and wear resistance, where an 0.88% attenuation rate reveals relatively weak transmittance stability under dust impact. Although the latter three attenuation rates are relatively higher, they still fall within an acceptable range compared to the long-term performance requirements of photovoltaic glass, and no significant deterioration in light transmittance performance caused by specific environmental aging tests was observed. Overall, the photovoltaic glass with TMOS exhibited excellent effective transmittance performance under various environmental aging test conditions, with no obvious performance differences between different tests. This indicates that the glass possesses favorable anti-aging capability and stability of light transmittance performance, providing strong data support for its long-term reliable application in complex outdoor environments.

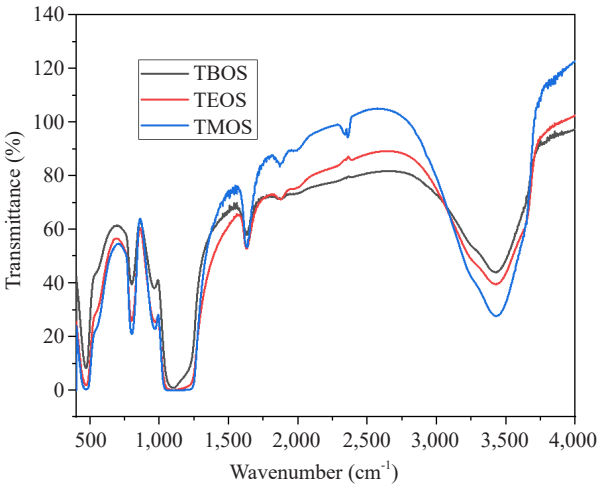

Figure 6. Infrared spectra of three samples

The absorption peak intensity of TMOS is the highest overall, especially the vibrational peaks in the range of 500 ~ 4,000 cm^{-1} (such as asymmetric stretching vibration of Si-O-Si, hydroxyl vibration, etc.) show the most significant response (Figure 6), indicating that its Si-O bond has strong vibrational activity, or the order and density of the silicon-oxygen network in the sample are relatively high. The intensity of TEOS is the second highest. The relative proportion of each characteristic peak is different from that of the blue line (TMOS), which may correspond to different Si-O bonding environments (such as the connection mode of silicon-oxygen tetrahedrons and the degree of defects). The intensity of TBOS is the lowest, suggesting that its silicon-oxygen structure has low compactness and functional group density, or there are many structural defects.

Combined with the molecular structure (Figure 7) of silicate precursors and XRD/SEM characterization results (Figures 1 and 2), TMOS with a shorter carbon chain exhibits less steric hindrance around its silicon center and lower activation energy for hydrolysis-condensation reactions, enabling rapid and uniform formation of an ordered Si-O-Si network. This is consistent with the previously observed higher crystallinity and dense microstructure; in contrast, TEOS and TBOS with longer carbon chains show increased steric hindrance and higher activation energy, leading to incomplete hydrolysis-condensation reactions. Ultimately, defective and loose structures are formed, with crystallinity significantly lower than that of TMOS.

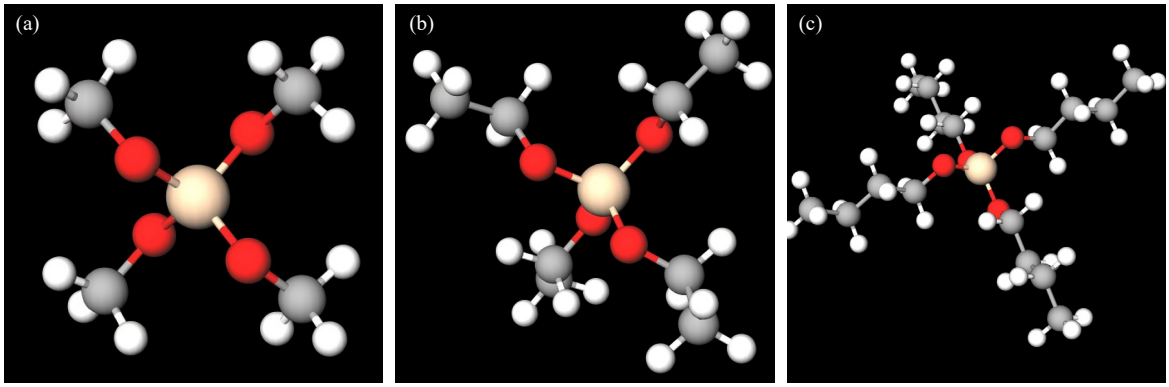

Figure 7. Molecular Structure of TMOS (a), TEOS (b), and TBOS (c)

Compared with the MgF_2/ZnS double-layer coating by Ding et al.,[15] the TMOS-based coating in this study achieves a higher visible light transmittance (up to 96%) and a lower IR transmittance (~ 40%), demonstrating superior synergistic performance in antireflection and infrared shielding. In terms of environmental stability, the TMOS coating exhibits an ultra-low transmittance attenuation rate of 0.02% under UV15 aging, which is significantly lower than that of the chitin nanofiber composite coating by Zhang et al.,[16] highlighting its outstanding long-term optical stability for outdoor applications. However, the TMOS coating shows a relatively higher attenuation rate (0.88%) under dust abrasion compared to the all-inorganic porous coating by Ji et al.,[17] indicating that its mechanical wear resistance still has room for improvement, which can be addressed through composite modification or process optimization in future work.

4. Conclusion

This study addresses solar energy loss from Photovoltaic (PV) glass reflection and efficiency degradation due to Infrared (IR) thermal effects, investigating the influence of silicate precursors with varying carbon chain lengths (TMOS, TEOS, TBOS) on PV glass coating performance. XRD and SEM show TMOS coatings exhibit higher crystallinity and denser, smoother microstructures, while TEOS/TBOS form rough, porous structures due to longer chains. Optical tests reveal TMOS coatings achieve the highest visible light transmittance (up to 96%) and lowest IR transmittance (~ 40%), demonstrating optimal light regulation. After 24-month stability and simulated aging tests, TMOS coatings show ultra-low transmittance attenuation (e.g., 0.02% under UV15), confirming excellent anti-aging durability. The study confirms short-chain TMOS as the optimal precursor for high-performance PV glass anti-reflection coatings, offering a viable solution to enhance PV system efficiency and longevity.

Acknowledgement

This work was supported by the National Natural Science Foundation of China (22578449), Fuzhou Major Science and Technology Project (2024-ZD-010), Fujian Provincial Science and Technology Project (2025H6017), Fujian Provincial Young and Middle-aged Teachers' Educational Research Project (JZ240045), and Fujian Provincial Natural Science Foundation (2025J08245).

Conflict of interest

The authors declare no competing financial interest.

Reference

[1] Du, Y.; Luna, L.; Tan, W. S.; Rubner, M. F.; Cohen, R. E. Hollow silica nanoparticles in UV-visible antireflection coatings for poly(methyl methacrylate) substrates. *ACS Nano* **2010,** *4*, 4308-4316.

[2] Wang, Q.; Wang, K.; Wang, M.; Wang, L.; Liu, H.; Zhang, W.; Li, D. The performance of laser-induced damage of a 2-4 μm mid-infrared anti-reflective coating based on HfO_2/SiO_2 materials. *Infrared Phys. Technol*. **2025,** *147*, 105771.

[3] Zhuang, K.; Chen, G.; Wang, Y.; Li, W.; Zheng, Y.; He, Z.; Zhao, Z.; Gao, M.; Chai,Y.; Peng, J. Phase-separation induced by retired photovoltaic glass enhances the quality of ferrosilicon alloy prepared from silicon powder waste. *Chem. Eng. J.* **2025,** *526*, 168454-168464.

[4] Yao, S.; Chen, H.; Dou, W.; Chen, Y.; Li, J.; Yu K. Failure analysis of micro-textured protrusions to photovoltaic glass surface under particle impact. *Eng. Fail. Anal.* **2025,** *181*, 109929-1099334.

[5] Wang, Y.; Li, S.; Tian, X.; Liu, Y.; Gao, L.; Feng, X.; Ma, Z. Sol-gel derived multilayer antireflective coatings fabricated at room temperature using nonthermal oxygen plasma. *Ceram. Int.* **2025,** *51*(18), 27081-27087.

[6] Oh, S.; Cho, J. W.; Lee, J.; Han, J.; Kim, S. K.; Nam, Y. A scalable haze-free antireflective hierarchical surface with self-cleaning capability. *Adv. Sci.* **2022,** *9*(27), 2202781.

[7] Huang, S.; Ma, Y.; Li, L.; Tu, J.; Yu, J.; Lei, L.; Luo, H.; He, Y.; Hou, J.; Kong, L.; et al. Effect of UV irradiation on SiN_x anti-reflective coating and silicon-based materials. *Sol. Energy Mater. Sol. Cells* **2025,** *289*, 113693.

[8] Wang, C.; Lu, K.; Li, C.; Ma, L.; Li, X.; Zhou, Y. Machine learning-assisted design of visibly transparent difunctional coatings for solar cell coloring and anti-reflection. *Renew. Energy* **2025,** *249*, 123160.

[9] Sarkın, A. S.; Ekren, N.; Sağlam, Ş. A review of anti-reflection and self-cleaning coatings on photovoltaic panels. *Sol. Energy* **2020,** *199*, 63-73.

[10] Tsoy, N.; Prado, V.; Wypkema, A.; Quist, J.; Mourad, M. Anticipatory life cycle assessment of sol-gel derived anti-reflective coating for greenhouse glass. *J. Clean. Prod.* **2019,** *221*, 365-376.

[11] Wang, X.; Wang, W.; Liu, J.; Qi, J.; He, Y.; Wang, Y.; Hu, W.; Cheng, Y.; Chen, K.; Hu, Y.; et al. Reducing optical reflection loss for Perovskite solar cells via printable mesoporous SiO_2 antireflection coatings. *Adv. Funct. Mater.* **2022,** *32*, 2203872.

[12] Xiao, L.; Li, Y.; Zhang, H.; Huang, G.; Cheng, Q.; Li, S.; Zhang, Y.; Zhou, H. Semitransparent organic solar cells with homogeneous transmission and colorful reflection enabled by an ITO-free microcavity architecture. *Adv. Mater.* **2023,** *36*, 2303844.

[13] Zhang, L.; Ren, L.; Song, W.; Wu, N.; Wang, S.; He, Q.; Zhang, Q. Scalable, robust, omnidirectional antireflective, superhydrophobic coatings based on chitin nanofibers for efficient solar energy collection. *Carbohydr. Polym.* **2025,** *359*, 123569.

[14] Zou, X.; Zhou, G.; Wan, Y.; Li, B.; Jiang, B.; Yan, H.; Wang, F. Designing multifunctional silica coatings for enhanced broadband antireflection and microfiber contamination sensing. *Chem. Eng. J.* **2023,** *473*, 145234.

[15] Ding, K.; Zhang, X.; Ning, L.; Shao, Z.; Xiao, P.; Ho-Baillie, A.; Zhang, X.; Jie, J. Hue tunable, high color saturation and high-efficiency graphene/silicon heterojunction solar cells with MgF_2/ZnS double anti-reflection layer. *Nano Energy* **2018,** *46*, 257-265.

[16] Casariego, P.; Sarrablo, V.; Barrientos, R.; Ibraikkulov, O. A.; Cros, S. Second photovoltaic prototype for textile ceramic technology: The perovskite glass solar brick. *Constr. Build. Mater.* **2025,** *493*, 143143-143149.

[17] Ji, C.; Zhang, Z.; Song, W.; Khalil, D. O.; Diana, B.; Byeongdu, L.; Ralu, D.; Supratik G.; Elena V. S. Porous but mechanically robust all-inorganic antireflective coatings synthesized using polymers of intrinsic microporosity. *ACS Nano* **2022,** *16*(9), 14754-14764.